Fretting Corrosion Behavior of Additive Manufactured and Cryogenic-Machined Ti6Al4V for Biomedical Applications

ADVANCED ENGINEERING MATERIALS

DOI: 10.1002/adem.201500629

Fretting Corrosion Behavior of Additive Manufactured and Cryogenic-Machined Ti6Al4V for Biomedical Applications

By *Rachele Bertolini,* Stefania Bruschi, Alberto Bordin, Andrea Ghiotti, Luca Pezzato* and *Manuele Dabalà*

Metal ion release, caused by synergistic effect of wear and corrosion, is one of the major concerns related to the prostheses lifetime. In this work, samples of additive manufactured Ti6Al4V are machined under dry cutting and cryogenic cooling conditions and their performances in terms of corrosion and fretting corrosion response are investigated. A wet and temperature-controlled apparatus equipped with an electro-chemical cell is designed and set-up in order to evaluate the fretting corrosion effect acting at the interfaces. The obtained results show that the cryogenic machining improves the corrosion and fretting corrosion behavior of the investigated additive manufactured Ti6Al4V.

1. Introduction

Fretting is defined to occur when two contacting surfaces are subjected to reciprocating motion of small displacement amplitude in the order of microns, whereas the conventional reciprocating motion relative to wear is known to occur at much larger displacement amplitude,[1] namely higher than 300 μm.[2,3] In case of biomedical applications, such as head-neck junction of hip prostheses, fretting at interfaces is usually accompanied by corrosion phenomena due to the fact that the mating surfaces are also exposed to body fluids that are known to be corrosive.[4–7] The simultaneous mechanical and electro-chemical phenomena taking place in the contact zone do not act independently, but depend on each other in a complex manner.[8] In such conditions, debris formation and metal ion release as a consequence of the wear phenomena can generate a localized anti-inflammatory response that is characterized by the formation of a fibrous tissue that encapsulates the implant. This triggers the osteolysis at the contact area between the bone and the implant,[9–12] which may lead to aseptic loosening, the major issue concerning the long-term outcome of a total hip arthroplasty.

Fretting corrosion is therefore a widespread concern in the orthopedic surgery and significant efforts have been recently made in understanding the involved factors as witnessed by several literature records.[13,14] However, besides the improvement in the knowledge about the interacting phenomena, the study of possible solutions to overcome the problem becomes mandatory to improve the effectiveness and long-term duration of the implants subjected to fretting corrosion.

With this in mind, the main objective of the present study is to evaluate the corrosion and fretting corrosion behavior of Ti6Al4V samples made of Additive Manufacturing (AM) and machined under dry cutting and cryogenic cooling conditions, the latter recently having proved to ameliorate the surface properties of the machined material.[15–17] The Ti6Al4V titanium alloy was chosen in the study as is the metal alloy conventionally used for biomedical applications because of its excellent characteristics of biocompatibility and corrosion resistance.[18–20] As counterpart material for the fretting corrosion experiments, the CoCrMo cobalt alloy was chosen in order to reproduce a common head-neck junction of femoral stems.[21,22]

Polarization scan, fretting corrosion tests, chemical analysis, and scanning electron microscopy analyses were used to examine the tribological and chemical behavior of AM Ti6Al4V samples. It was proved that machining under cryogenic cooling improves the corrosion and fretting corrosion characteristics of Ti6Al4V samples compared to dry cutting.

2. Materials and Methods

2.1. Materials

The materials chosen in this study as the basis for the research and representative of the artificial joint heads and neck pair are the Ti6Al4V alloy and the CoCrMo alloy.[6,23]

[*] *Dr. R. Bertolini, Prof. S. Bruschi, Dr. A. Bordin, Prof. A. Ghiotti*
Department of Industrial Engineering, University of Padova, Via Venezia 1, 35131 Padova, Italy
E-mail: rachele.bertolini@dii.unipd.it
Dr. L. Pezzato, Prof. M. Dabalà
Department of Industrial Engineering, University of Padova, Via Marzolo 9, 35131 Padova, Italy

The Ti6Al4V was produced in the form of cylindrical billets manufactured through the Electron Beam Melting (EBM) AM technology using an ARCAM Q10 machine. Each billet was manufactured with the symmetry axis parallel to the growing direction, with a diameter of 24 mm and a height of 180 mm.

Ti6Al4V pins were machined in cylindrical shape and with a diameter of 20 (±0.02) mm and a length of 5 (±0.02) mm.

The counterpart material is the wrought ASTM F1537 CoCrMo cobalt alloy, provided in form of a 29 mm diameter round bar that was machined into plates with a nominal edge of 20 mm and a thickness equal to 3 mm. After milling, the plates were ground achieving a planarity tolerance of 0.005 mm.

The plates had a final area of 20×20 (±0.02) mm^2 and a thickness of 2 (±0.02) mm.

Different CoCrMo flat plates were used for each tribology test in order to not alter the results.

The chemical compositions of the two alloys and their main mechanical properties are shown in Table 1.[24,25]

2.2. Machining Tests

A Mori Seiki lathe, equipped with a special designed line to fulfill cryogenic cooling, was used to carry out the turning operations to machine the Ti6Al4V pins. Liquid Nitrogen (LN2) was sprayed toward the tool flank and rake faces using two copper nozzles with an internal diameter of 0.9 mm, according to the experimental set-up reported in a previous work.[26] The cryogenic fluid was sprayed onto the workpiece surface using a vacuum-insulated pipe at a pressure of 6 bars.

The used cutting tool was a DNMG 15604 SM H13A with a radius of 0.4 mm, mounted on a PDJNR 2020K15 tool holder with an approach angle of 93°, both provided by Sandvik Coromant.

The cutting tests were run with different cutting speed (v_c), namely 50 and 80 m min^{-1}, feed rate (f), namely 0.1 and 0.2 mm rev^{-1}, and cutting conditions, namely in dry and cryogenic conditions. Each condition was properly selected to be representative of the real scenario that could be encountered in machining biomedical devices. The depth of cut (d) was maintained constant and equal to 0.25 mm, therefore the cutting tests were performed within semi-finishing cutting conditions. In order to assure repeatability of the results, two cylindrical pins were realized for each cutting condition.

Table 1. Mechanical properties and chemical composition[24,25] of the EBM Ti6Al4V and ASTM F1537 CoCrMo.

	EBM Ti6Al4V	ASTM F1537 CoCrMo
Elastic modulus, E [GPa]	120	240
Yield strength, Y [MPa]	950	827
Ultimate tensile strength, UTS [MPa]	1 020	1 172
Hardness, HRC [HRC]	33	35
Elongation	14%	12%
Chemical composition, [weight %]	Ti 89.7% Al 6% V 4% C 0.03% O 0.15% Fe 0.1% N 0.01% H 0.003%	Co 64.86% Cr 26% Mo 6% C 0.14% Fe 0.75% Ni 1% N 0.25% Si ≤ 1%

Taking into account that the AM technologies[27] require a machining allowance left on the raw workpiece in the range between 0.1 and 0.25 mm, the machining steps to obtain the final shape were minimized. Pre-turning operations were made in order to achieve a diameter of 21 mm, leaving a machining allowance of 0.5 mm on the radius of the raw samples. In this way, the requirements of the AM technologies were satisfied. The cylindrical specimens were reduced from a diameter of 24 mm to a diameter of 21 mm in dry conditions. Afterward, the pre-turned samples were clamped only at the spindle assuring a maximum unsupported length of 30 mm with the aim to reduce vibrations. After machining, a cutting-off operation was carried out in order to achieve the final length of 5 mm.

2.3. Surface Characterization of the Machined Samples

The Ti6Al4V pins surface characterization was performed through micro-hardness and residual stresses measurements after semi-finishing turning.

Vickers micro indentation tests were carried out by using a Leitz Durimet micro-hardness tester with a load of 50 g for 30 s; five values were recorded for each cylindrical pin and then the average value calculated.

XRD analysis was carried out on an Enixè TNX diffractometer in order to investigate the microstructural alterations under the machined surfaces. The xrd- $\sin^2\psi$ method[28] was employed using CuKα radiation at 85 μA. A number of nine tilt angles (ψ) were employed.

The residual stresses along the axial and circumferential directions with respect to the cylindrical pin axis were measured on the surface and at a depth of 25 μm below the surface, by removing the material layers through an electro-polishing process to avoid modifications of the machining-induced stresses.

2.4. Corrosion Tests

The potentiodynamic polarization curves were obtained through testing in a 9 g L^{-1} of NaCl solution at body temperature (37 ± 1 °C), using an Amel 2549 potentiostat.

A standard three-electrode corrosion cell with an electrolyte volume of 800 mL was used for the electrochemical measurements, where the Saturated Calomel Electrode (SCE) was used as the reference electrode and a platinum electrode as the counter electrode. The active area of the Ti6Al4V electrode was 5.625 cm^2. Potentiodynamic polarizations were performed by using an initial delay time at equilibrium state of 60 min in order to stabilize the surface at Open Circuit Potential (OPC). The recording of the potential started at

DOI: 10.1002/adem.201500629

−0.8 V and finished at +1.2 V, according to the ASTM G5-14 standard. A potential scan rate of 0.5 mV s^{-1} was used.

2.5. Fretting Corrosion Tests

The fretting corrosion tests were carried out on an Rtec Instruments tribometer using a newly developed apparatus. The employed contact configuration consisted in a Ti6Al4V cylindrical pin, mounted on a non-conductive holder, sliding against an underlying CoCrMo plate. Such type of configuration was selected as it was the most suitable to investigate the behavior of cylindrical shapes obtained by turning.[29,30]

The shape and dimensions of the cylindrical pins were selected in order to generate the same level of contact pressure found by a non-linear 3-D Finite Element (FE) stress analysis carried out to determine the contact loads at the interfaces between the neck and femoral head (see Section 2.5.1).

The contact interface was immersed in a 0.9% saline solution constantly maintained at a temperature of 37 ± 1 °C. A thermometer, immersed in the water basin, was used in order to have a feedback of the temperature in the solution. The experiments were performed at a frequency of 1 Hz, in order to replicate the average frequency of human walking,[31] and lasted 3 600 s. The displacement amplitude was set equal to 100 μm; therefore, tests were performed within the gross-slip regime.[2]

A three-electrode electro-chemical cell, the same one used for the corrosion tests, was integrated into the system to perform the fretting corrosion tests. The working electrode, properly isolated on the lateral surfaces, was embedded in a non-conductive pin-holder. The voltage of the pump, which raises the liquid in the water basin, was maintained constant in order to avoid fluctuation of the level of the saline solution. The schematic view of the fretting corrosion experimental set-up is shown in Figure 1.

The OCP was measured as a function of the time. The test consisted in two different phases: first, the pin was immersed in static conditions for 120 s, then the specific load was applied and the actual fretting test started and lasted 3 600 s. Finally, the test was stopped and the pin unloaded.

2.5.1. Contact Pressure Estimation

The test loading conditions for the fretting corrosion tests were chosen based on a non-linear 3-D Finite Element (FE) stress analysis carried out to determine the contact load at the interface between the neck and femoral head. The FE model was developed in PTC Creo Parametric by modeling the stem neck with tetrahedral solid elements of an average element size of 0.5 mm, while the stem and head prosthesis were meshed using tetrahedral solid elements of an average size of 2 mm. A 3 000 N load was applied at the center of the femoral head, following the ISO 7206–7 standard recommendations. A maximum tensile stress equal to 100 MPa was calculated, in close agreement with the findings of another numerical study.[29]

The Hertzian contact theory was used to calculate the maximum contact pressure for the given cylinder-on-plane contact by using Equation 1:

$$F = \frac{P_{MAX} \times L \times b \times \pi}{2} \quad (1)$$

where P_{MAX} is the maximum contact pressure, F the normal load applied to the surface, L the length of contact, and b the half width of the rectangular contact area. The equation of "b" and the explanation of its parameters can be found in a previous work.[32]

The values of the Poisson's ratio for evaluating "b" is assumed to be 0.34 for both the materials.[29]

The radius of the plate specimen was infinite (being a plane surface), whereas the radius of the cylindrical pin was equal to 10 mm. The length of the pin was chosen in order to replicate the results of the 3-D FE stress analysis following the Hertz's theory. The force calculated in order to obtain the maximum contact pressure of 100 MPa resulted in 18 N.

2.6. Wear Characterization

After the fretting corrosion tests, the Ti6Al4V pins were ultrasonically cleaned in acetone for 10 min and the worn surfaces were analyzed using an FEI QUANTA 450 TM Scanning Electron Microscope (SEM) equipped with the Everhart-Thornley Detector (ETD) and Backscattered Electron (BSED) detectors. Furthermore, the energy dispersive X-ray analysis (EDX) was carried out to identify the surface chemical composition.

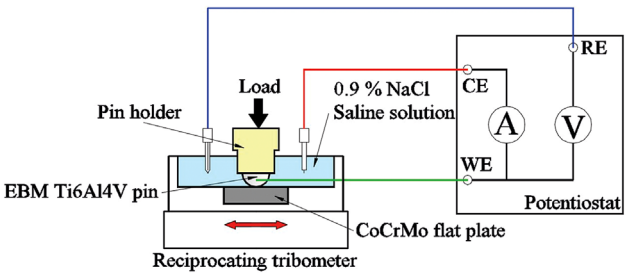

Fig. 1. Scheme of the experimental set up for the fretting corrosion tests.

3. Results

3.1. Characteristics of the Machined Samples

Table 2 reports both the residual stresses and micro-hardness values as a function of the different cutting conditions.

Micro-hardness of the pins, before machining, was 335 ± 4 $HV_{0.05}$.

Compared to the micro-hardness of the dry-machined pins, an increase of up to 8% was achieved after cryogenic machining. Moreover, with the same machining conditions, the application of liquid nitrogen led to higher compressive residual stresses, improving the surface conditions of the investigated Ti6Al4V pins. These experimental findings are confirmed by several authors who have studied the possible benefits of the applications of LN2.

Table 2. Surface integrity of the EBM Ti6Al4V pins after the semi-finishing turning process.

Cutting parameters			Micro-hardness	Residual stresses			
V_c [m min^{-1}]	f [mm rev^{-1}]	Cutting condition	$Hv_{0.05}$	σa_s [MPa]	σa_d [MPa]	σt_s [MPa]	σt_d [MPa]
50	0.1	Dry	378 ± 6	−64	−15	−276	−149
50	0.2	Dry	371.8 ± 7	−80	−20	−214	−150
80	0.1	Dry	369 ± 4	−28	49	−205	−250
80	0.2	Dry	367.1 ± 4	14	31	−264	−232
50	0.1	Cryogenic	409.4 ± 8	−123	−156	−156	−80
50	0.2	Cryogenic	389 ± 7	−152	−42	−307	37
80	0.1	Cryogenic	400.2 ± 5	−87	20	−148	−90
80	0.2	Cryogenic	385 ± 5	−69	−32	−354	−235

[σa]: residual stress along the axial direction; [σt]: residual stress along the tangential direction; [σx_s]: residual stresses measured on the surface (depth = 0 μm); [σx_d]: residual stresses measured at a depth of 25 μm below the surface.

Jawahir and coworkers[33] demonstrate that a significant improvement in terms of superficial hardness, which leads to enhanced corrosion properties, can be achieved adopting cryogenic-assisted machining.

Pu et al.[34] proved that the cryogenic cooling may represent an efficient method to improve the product functional properties, as it leads to both hardness increase and compressive residual stresses along the axial direction in machining the AZ31B magnesium alloy.

In this way, cryogenic machining may substitute surface treatments aimed at improving both the fatigue and wear resistance as shot peening and electro-polishing.

3.2. Corrosion Behavior

The polarization curves of the EBM TiAl4V samples machined at a cutting speed equal to 50 and 80 m min^{-1} are given in Figure 2a and b, respectively. The obtained values of the corrosion potentials and corrosion current densities are summarized in Table 3.

Table 3 and Figure 2 show that machining the EBM Ti6Al4V under cryogenic cooling conditions produces an ennoblement of the samples compared to the dry-machined ones as, regardless the cutting parameters, all the cryogenic-machined samples present curves that are shifted toward higher potentials.

The highest potential values were observed for the pins obtained in cryogenic conditions and machined with a feed rate equal to 0.2 mm rev^{-1}, with an ennoblement of about 0.25 V for a cutting speed of 50 m min^{-1}, and an ennoblement equal to 0.14 V for a cutting speed of 80 m min^{-1}.

In terms of corrosion current density, which is directly connected with the corrosion rate through the Faraday law, there are no significant differences between the samples machined in dry and cryogenic conditions except for the pins machined with the most severe parameters. In fact for these samples, a reduction of about one order of magnitude in the

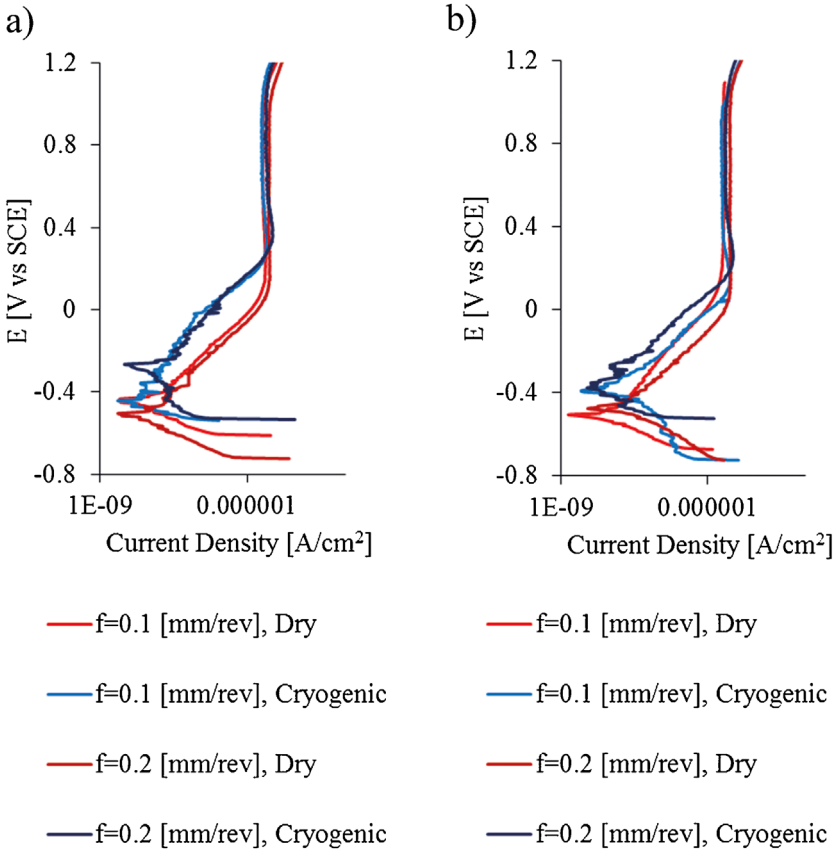

Fig. 2. Influence of the cutting speed on the anodic polarization plot of EBM Ti6Al4V pins corroded in saline solution at body temperature: (a) cutting speed of 50 m min^{-1}; (b) cutting speed of 80 m min^{-1}.

ADVANCED ENGINEERING MATERIALS 2016,
DOI: 10.1002/adem.201500629

ADVANCED ENGINEERING MATERIALS

Table 3. Current density and corrosion potential of the EBM Ti6Al4V pins corroded in saline solution at body temperature as a function of the cutting parameters.

V_c [m min^{-1}]	f [mm rev^{-1}]	Cutting condition	E_{corr} [V]	I_{corr} [mA cm^{-2}]
50	0.1	Dry	−0.45	0.02
50	0.2	Dry	−0.53	0.01
80	0.1	Dry	−0.55	0.03
80	0.2	Dry	−0.5	0.1
50	0.1	Cryogenic	−0.45	0.01
50	0.2	Cryogenic	−0.28	0.01
80	0.1	Cryogenic	−0.4	0.03
80	0.2	Cryogenic	−0.36	0.01

corrosion current density can be observed if compared with the pins machined in dry conditions.

This indicates that the corrosion properties are strongly influenced by the turning process parameters, and opens a new scenario, namely machining under cryogenic cooling conditions and adopting severe cutting parameters can lead to a significant reduction in the corrosion rate.

The data reported in Table 3 indicate that the cryogenic cooling produces a positive effect compared to dry cutting by mostly increasing the corrosion potential and in one case greatly reducing the current density. This behavior can be ascribed to the enhanced surface properties and, in particular, with the high compressive tensile state recorded with the XRD residual stress measurements on the surface of the pins machined in cryogenic conditions, as reported in Table 2. The strong correlation between the compressive residual stresses and the improved corrosion performances can be found in the literature. Wan[35] found a close connection between the residual stresses and the corrosion resistance, claiming that the increase of the compressive superficial stress state leads to a decrease in the damage extent provoked by the corrosion phenomena. Also Takakuwa and Soyama[36] demonstrated the influence of the residual stress state on the corrosion behavior of an austenitic stainless steel, showing that the polarization curves are strongly affected by the surface characteristics.

Therefore, considering that there is a strong correlation between the machining conditions and the induced residual stresses, as demonstrated by the data reported in Table 2, it can be stated that the machining parameters can greatly affect the material properties and its ability to withstand to corrosive media. In particular, it was here demonstrated that machining in cryogenic conditions improves the corrosion resistance of the EBM Ti6Al4V.

3.3. Open Circuit Potential (OCP) Measurements

The outcomes of the OCP measurements during the fretting corrosion tests are shown in Figure 3. In the first 120 s before the application of the load, the OCP values increase suggesting a thickening of the passive layer. After these first 120 s, fretting test started and the OCP values dropped toward more active values. The OCP reached a minimum value immediately after the beginning of sliding and tended to increase toward less active values due to the equilibrium between the mechanical depassivation and electro-chemical repassivation.

During sliding, the OCP values tend to present a slight increment as seen in a previous work.[37] The values of the maximum variation of the OCP (named ΔE_{MAX}) and the value of the potential assumed by the pins during the test (named E_{AVG}) are shown in Table 4. In general, the initial depassivation peak (ΔE_{MAX}) was more prominent in the case of cryogenic-machined pins. This fact can be explained with the surface properties of the cryogenic-machined pins: when sliding began and the pin started to rub against the plate, the initial destruction of the passive layer is more significant in the cryogenic-machined surface, because this one is harder and more brittle compared with the one of the dry-machined pins, as reported in Table 2.

After the initial cathodic peak, the average values of the potential assumed by the cryogenic-machined pins were generally arranged at a higher level compared to the dry-machined pins.

This fact indicates improved tribo-corrosion performances of the cryogenic-machined pins and is in accordance with the results of the potentiodynamic polarization test previously reported.

The greatest differences can be found on those curves that characterize the pins machined at a feed rate equal to 0.1 mm

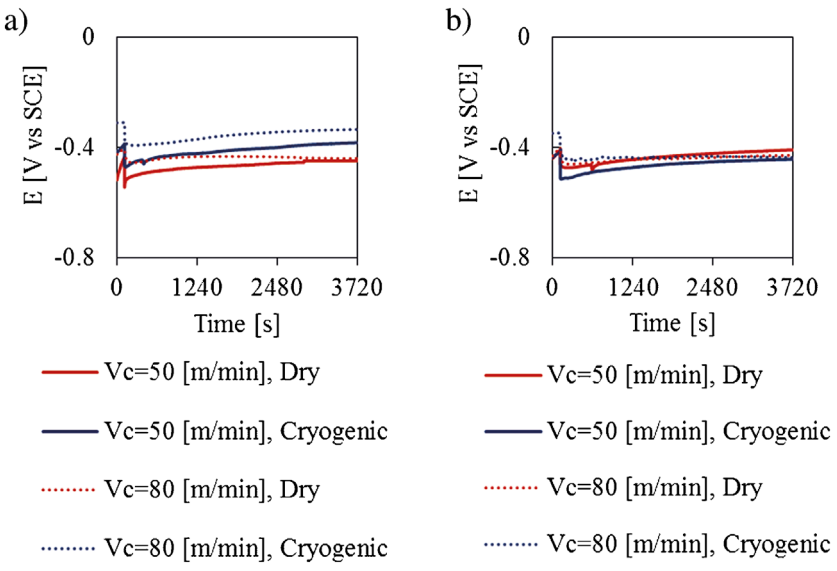

Fig. 3. Influence of the feed rate on the evolution of the OCP for the EBM Ti6Al4V pins in 0.9% NaCl solution at body temperature; (a) feed rate equal to 0.1 mm rev^{-1}; (b) feed rate equal to 0.2 mm rev^{-1}.

DOI: 10.1002/adem.201500629

Table 4. Average values of the COF, maximum drop (ΔE_{MAX}), and average value (E_{AVG}) of the potential assumed by the EBM Ti6Al4V pins as a function of the cutting parameters.

V_c [m min^{-1}]	f [mm rev^{-1}]	Cutting condition	E_{AVG} [V]	ΔE_{MAX} [mV]	Average COF
50	0.1	Dry	−0.46	84 ± 22	0.13 ± 0.08
50	0.2	Dry	−0.43	99 ± 30	0.11 ± 0.08
80	0.1	Dry	−0.43	52 ± 10	0.11 ± 0.07
80	0.2	Dry	−0.45	30 ± 14	0.16 ± 0.09
50	0.1	Cryogenic	−0.41	109 ± 5	0.12 ± 0.07
50	0.2	Cryogenic	−0.46	78 ± 13	0.20 ± 0.09
80	0.1	Cryogenic	−0.35	83 ± 7	0.08 ± 0.02
80	0.2	Cryogenic	−0.42	106 ± 9	0.08 ± 0.03

rev^{-1}: indeed from Figure 3, it can be seen that they are shifted toward significantly less negative values.

The only exception can be detected for the pin machined under cryogenic cooling condition at $V_c = 50\,\text{m min}^{-1}$ and $f = 0.2\,\text{m min}^{-1}$: its plot stabilizes around a lower level compared to the corresponding dry one. Fretting corrosion phenomena is a synergistic combination of wear and corrosion: in this case, the mechanical aspects may assume the major contribution compared to the chemical one. In fact, the pin machined at cutting speed equal to 50 m min^{-1} and feed rate equal to 0.2 mm rev^{-1} has lower increase of hardness compared to the cryogenic pins obtained in the other conditions, leading to a more severe wear and therefore to a fretting corrosion curve shifted toward more negative values. This can be due to the fact that these cutting conditions are intermediate between the least and the most severe ones and the effect of using LN2 as cooling medium may be less influential than in the other cases.

Summarizing in general, a positive influence of the cryogenic machining on fretting corrosion behavior can be highlighted, which can be ascribed to both improved surface characteristics and corrosion behavior.

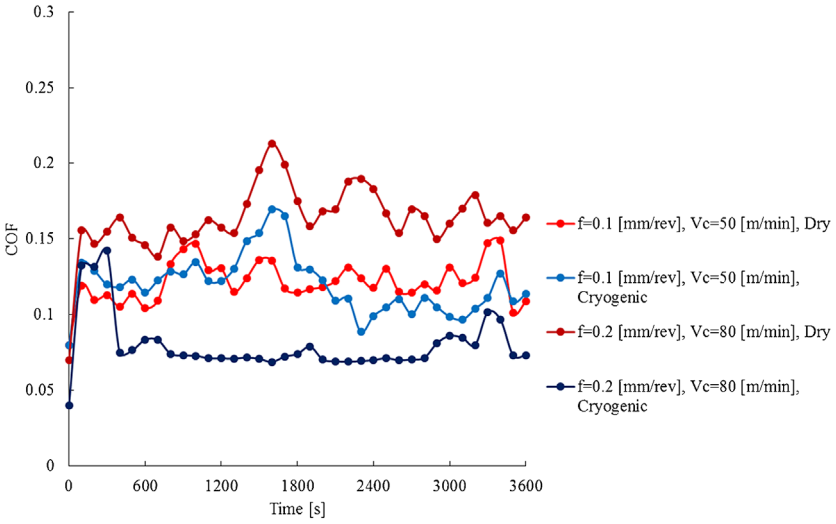

Fig. 4. Evolution of the COF for the EBM Ti6Al4V pins machined at different cutting parameters.

3.4. Coefficient of Friction (COF)

The evolution of the COF as a function of the time is shown on Figure 4 for the least and most severe cutting parameters adopted in the experimental plan. The COF increases rapidly during the first seconds of the test and then tends to fluctuate around a stable value.

As can be seen from Figure 4, the friction curves for the cryogenic pins always lie at a lower level, being very significant especially in the case of the most severe cutting parameters. The measured average values of the COF are listed in Table 4, where it is evident that, regardless of the cutting parameters, the COF for the cryogenic-machined pins is always lower as a consequence of a more hardened surface layer provoked by the cryogenic machining in accordance with the Archard's law.

The only exception is represented by the pin machined in cryogenic conditions with a feed rate equal to 0.2 mm rev^{-1} and cutting speed equal to 50 m min^{-1}.

3.5. Wear Analysis

The worn surfaces of the EBM Ti6Al4V pins after fretting corrosion tests are characterized by two main different wear mechanisms namely abrasive and adhesive wear. Abrasive wear is represented by the parallel grooves left on the pin surfaces due to the sliding against the CoCrMo plate.

Adhesive wear is characterized by the presence of counterpart material on the pin surface, due to the repetitive scratching of the mating surfaces during sliding that led to material removal.

SEM-magnified images of the machined feed marks are shown in Figure 5, together with the chemical elements maps obtained by the EDX chemical analysis. The spectra are referred to a zone of investigation composed by a rectangle of a length equal to 58 pixels and a height equal to 50 pixels, placed in correspondence of the central feed marks of the wear scars.

The central area of the wear scar is subjected to much more intensive abrasion

DOI: 10.1002/adem.201500629

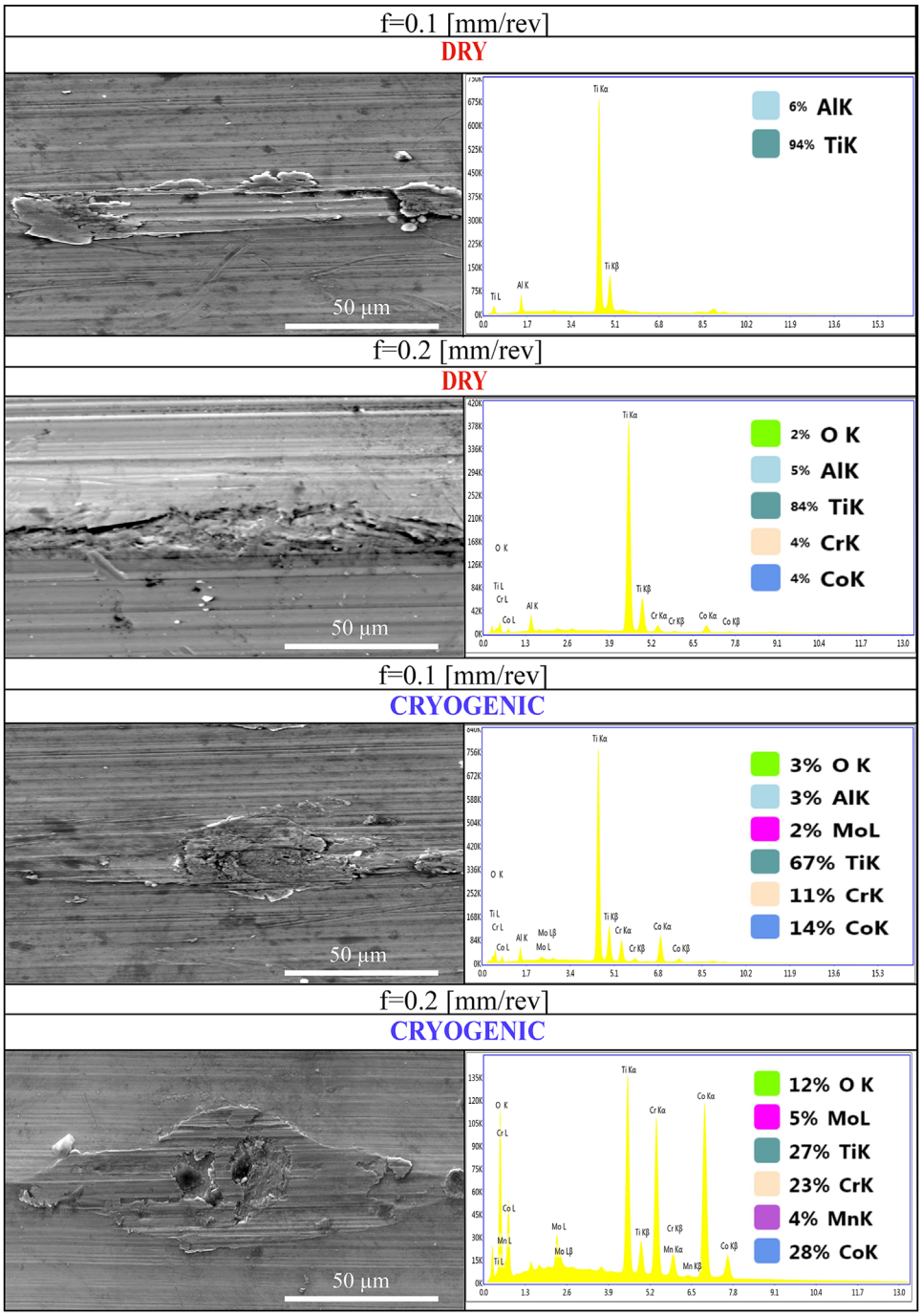

Fig. 5. SEM images of the worn surfaces and relative chemical analysis for the EBM Ti6Al4V pins machined at a cutting speed of 50 m min^{-1}.

compared to the external zones, which are characterized by material accumulation.

The chemical maps suggest that the percentage of elements adhered on the cryogenic machined pins is higher compared to the dry-machined ones. This could be ascribed to the improved surface characteristics and to a less severe damage as a consequence of the corrosion medium. Higher amount of Co, Cr, and Mo are located on the EBM Ti6Al4V pins surfaces due to the repetitive material transfer from the counter material to the pin. The formation of an adhered layer can positively influence the wear behavior of the material protecting the underlying layers from further abrasive wear. This can lead to a less debris formation, which is one of the main concerns from the biomedical point of view, evidencing that cryogenic machining can be considered as an effective technology to machine medical prostheses.

Table 5. Summary of the effectiveness of adopting Liquid Nitrogen as cooling medium during semi-finishing machining.

Cutting Condition	Micro-hardness	Residual stresses	Corrosion properties	Fretting corrosion properties	COF	Adhesion from the counterpart material
Dry	Worse	Worse	Worse	Worse *	Worse *	Lower
Cryogenic	Improved	Improved	Improved	Improved *	Improved *	Higher

[*] Except for the pin machined at 0.2 mm rev^{-1} and 50 m min^{-1}.

4. Conclusions

The influence of the cutting parameters and lubricating strategies on the fretting corrosion behavior of the EBM Ti6Al4V alloy was investigated.

Fretting corrosion tests were carried in a newly developed experimental apparatus reproducing both contact and physical conditions similar to the taper interfaces of modular hip prostheses in human body.

Cryogenic machining appears as the most effective cutting strategy that can enhance the mechanical, chemical, and tribological behavior of the machined surfaces.

Table 5 summarizes the overall results, highlighting the positive and negative aspects of adopting dry cutting and cryogenic cooling.

Based on the results of this investigation, the following conclusions can be drawn:

1) Cryogenic-machined EBM Ti6Al4V pins are characterized by both higher micro-hardness values and higher compressive residual stresses compared to the dry-machined ones. The anodic polarization curves show that the cryogenic machining improves the corrosion behavior.
2) The OCP values of the cryogenic-machined pins recorded during the fretting tests are, in the most cases, arranged at a higher level compared to the dry-machined ones, meaning they are less affected by the surrounding corrosion medium. The average coefficient of friction of the cryogenic-machined pins settles to a lower value compared to the dry-machined ones.
3) The chemical analysis of the EBM Ti6Al4V pins worn surfaces shows an increase of the amount of chemical elements adhered on the pins from the counterpart material: this indicates a higher degree of adhesive wear that can protect the underlying material from further abrasive wear.

Article first published online: xxxx
Manuscript Revised: January 25, 2016
Manuscript Received: December 12, 2015

[1] G. X. Chen, Z. R. Zhou, *Wear* **2001**, *250–251*, 665.
[2] O. Vingsbo, S. Söderberg, *Wear* **1988**, *126*, 131.
[3] M. O. Alam, S. M. Haseeb, *Tribol. Int*. **2002**, *35*, 357.
[4] R. M. R. Dyrkacz, J. M. Brandt, O. A. Ojo, T. R. Turgeon, U. P. Wyss, *J. Arthroplasty* **2013**, *28*, 1036.
[5] S. Hussenbocus, D. Kosuge, L. B. Solomon, D. W. Howie, R. H. Oskouei, *BioMed. Res. Int*. **2015**, *2015*, 9.
[6] J. S. Kawalec, S. A. Brown, J. H. Payer, K. Merritt, *J. Biomed. Mater. Res*. **1995**, *29*, 867.
[7] G. B. Higgs, J. A. Hanzlik, D. W. MacDonald, W. M. Kane, J. S. Day, G. R. Klein, *ASTM Int*. **2013**, *1560*, 146.
[8] N. Diomidis, J. P. Celis, P. Ponthiaux, F. Wenger, *Wear* **2010**, *269*, 93.
[9] J. L. Gilbert, C. A. Buckley, J. J. Jacobs, *J. Biomed. Mater. Res*. **1993**, *27*, 1533.
[10] R. M. Urban, J. J. Jacobs, J. L. Gilbert, J. O. Galante, *J. Bone Jt. Surg. – Ser. A* **1994**, *76*, 1345.
[11] S. D. Cook, R. L. Barrack, G. C. Baffes, A. J. T. Clemow, P. Serekian, N. Dong, *Clin. Orthop. Relat. Res*. **1994**, *298*, 80.
[12] S. D. Cook, R. L. Barrack, A. J. T. Clemow, *J. Bone Jt. Surg. – Ser. B* **1994**, *76*, 68.
[13] D. Royhman, M. Patel, M. J. Runa, J. J. Jacobs, N. J. Halla, M. Wimmer, *Tribol. Int*. **2015**, *91*, 235.
[14] J. S. Rituerto, S. Suñer, A. Neville, N. Emami, *Tribol. Int*. **2014**, *75*, 10.
[15] A. Bordin, A. Ghiotti, S. Bruschi, L. Facchini, F. Bucciotti, *Procedia CIRP* **2014**, *14*, 89.
[16] A. Bordin, S. Bruschi, A. Ghiotti, P. F. Bariani, *Wear* **2015**, *328–329*, 89.
[17] S. Sartori, A. Bordin, S. Bruschi, A. Ghiotti, *Key Eng. Mater.* **2015**, *651–653*, 1183.
[18] M. C. García-Alonso, L. Saldaña, G. Vallés, J. L. González-Carrasco, J. González-Cabrero, M. E. Martínez, *Biomaterials* **2003**, *24*, 19.
[19] Y. Li, C. Yang, H. Zhao, S. Qu, X. Li, Y. Li, *Materials* **2014**, *7*, 1709.
[20] M. Long, H. J. Rack, *Biomaterials* **1998**, *19*, 1621.
[21] C. V. Vidal, A. I. Muñoz, *Corros. Sci*. **2008**, *50*, 1954.
[22] R. A. Gil, A. I. Muñoz, *J. Mech. Behav. Biomed. Mater.* **2011**, *4*, 2090.
[23] P. E. Sinnett-Jones, J. A. Wharton, R. J. K. Wood, *Wear* **2005**, *259*, 898.
[24] http://www.arcam.com/technology/electron-beam-melting/material

DOI: 10.1002/adem.201500629

[25] ASTM International, ASTM F1537-11, **2011**.
[26] M. J. Bermingham, S. Palanisamy, D. Kent, M. S. Dargusch, *J. Mater. Process. Technol*. **2012**, *212*, 752.
[27] F. H. Froes, B. Dutta, *Adv. Mater. Res*. **2014**, *1019*, 19.
[28] I. C. Noyan, J. B. Cohen, *Sagamore Army Mater. Res. Conf. Proc*., Plenum Press, New York, NY, USA **1982**, 1.
[29] T. Zhang, N. M. Harrison, P. F. McDonnell, P. E. McHugh, S. B. Leen, *Tribol. Int*. **2013**, *65*, 113.
[30] A. L. M. Tobi, J. Ding, G. Bandak, S. B. Leen, P. H. Shipway, *Wear* **2009**, *267*, 270.
[31] M. Baxmann, S. Y. Jauch, C. Schilling, W. Blömer, T. M. Grupp, M. M. Morlock, *Med. Eng. Phys*. **2013**, *35*, 676.
[32] T. Roy, D. Choudhury, S. Ghosh, A. B. Mamat, B. Pingguan-Murphy, *Ceram. Int*. **2015**, *41*, 681.
[33] F. Pusavec, H. Hamdi, J. Kopac, I. S. Jawahir, *J. Mater. Process Technol*. **2011**, *211*, 773.
[34] Z. Pu, J. C. Outeiro, A. C. Batista, O. W. Dillon, D. A. Puleo, I. S. Jawahir, *Int. J. Mach. Tools Manuf*. **2012**, *56*, 17.
[35] Y. Y. Wan, *Adv. Mater. Res*. **2014**, *1017*, 4.
[36] O. Takakuwa, H. Soyama, *Adv. Chem. Eng. Sci*. **2015**, *5*, 62.
[37] Z. Doni, A. C. Alves, F. Toptan, J. R. Gomes, A. Ramalho, M. Buciumeanu, *Mater. Des*. **2013**, *52*, 47.